Guerrero Garcia, J.M., Mayugo Majó, J.A., Costa i Balanzat, J., Turon Travesa, A. (2020). Failure of hybrid composites under longitudinal tension: influence of dynamic effects and thermal residual stresses. *Composite Structures*, vol. 233, art.num. 111732. DOI https://doi.org/10.1016/j.compstruct.2019.111732

Failure of hybrid composites under longitudinal tension: influence of dynamic effects and thermal residual stresses

Jose M. Guerrero[a,*], Joan A. Mayugo[a], Josep Costa[a], Albert Turon[a]

[a]AMADE, Polytechnic School, Universitat de Girona, Campus Montilivi s/n, E-17003 Girona, Spain

Abstract

A progressive failure model including dynamic effects and thermal residual stresses able to simulate the failure and damage development of hybrid unidirectional polymer composites under fibre tensile loading is presented. The model is used to study the influence dynamic effects and thermal residual stresses have on the development of clusters of fibre breaks and the failure process of different hybrid composites. The results obtained show that while the dynamic effects change cluster formation, nonetheless they do not significantly alter the final failure of the material. Overall, the influence is greater for the more brittle materials. Although the thermal residual stresses do not affect the formation of clusters, they can delay damage initiation and final failure by inducing compressive stresses into the fibres.

Keywords: Dynamic effects, Thermal residual stresses, Hybrid, Micro-mechanics

1. Introduction

Fibre hybridization, obtained by mixing a Low Elongation (LE) fibre with a High Elongation (HE) fibre in a single matrix, is a promising strategy that can overcome the inherent quasi-brittle behaviour and low toughness of Fibre Reinforced Polymers (FRP) that leads to fibre tensile failure with hardly any prior damage symptoms [1–5]. With a certain hybridization, the failure process of the material can be altered, leading to hybrid effects and an increase in ductility [3, 4, 6–16]. At present, changes in failure development, thermal residual stresses and dynamic effects are the main explanations for the so-called effects [6, 17–19].

*Corresponding author. Tel.: +34 972 41 88 17.
Email address: josemanuel.guerrero@udg.edu (Jose M. Guerrero)

The tensile strength of brittle fibres is not deterministic and can be characterized with a statistical distribution. When a fibre breaks, the fibre loses its load carrying capacity over a distance known as ineffective length. Along this length, the neighbouring intact fibres are subjected to stress concentrations. Intrinsically, this stress redistribution is dynamic. When a fibre fails, the strain energy sustained by the fibre is released in the form of a stress wave which dampens after some time. During this period, dynamic stress concentrations, which exceed the static, appear in intact fibres around the broken fibre [18, 20–24]. Currently, it has been reported that the dynamic stress concentration can be between 10% to 110% higher than the static depending on the configuration of the material [24]. As the load is increased, clusters of broken fibres start to form, which will eventually lead to final failure. It is, however, unclear if final failure is triggered due to the accumulation of damage or the unstable propagation of a large critical cluster [1]. In a non-hybrid composite this failure process occurs quickly, leading to a catastrophic failure. Nonetheless, in a hybrid composite, the formation of clusters can be altered thanks to the difference between the elastic and geometrical properties of the two fibre populations in the hybrid, leading to hybrid effects [3, 4, 7–9, 11, 15, 16].

Two main modelling approaches can be found in the literature to predict the fibre tensile failure of composites. Global Load Sharing (GLS) [2, 10, 11, 25–28], which cannot capture the formation of clusters, and Local Load Sharing (LLS) [3, 4, 8, 9, 11, 12, 24, 29–35] which are able to do so. In general, models can predict the failure strength within an accuracy of around 20%, but overpredict the fibre break density at failure and underpredict the formation of co-planar clusters. In addition, compared with experiments, most models predict the formation of larger clusters too late. These issues have been mainly attributed to the omission of the dynamic effects due to fibre failure [1, 3, 5, 36].

To study their importance, Bullegas [35], incorporated for the first time, the dynamic effects in the tensile failure process of non-hybrid composites using a simplified approach. A 10% decrease in strength was found. Moreover, the average distance between consecutive breaks decreased when using the dynamic model. Such findings should have made the modelling results closer to the experiments. Unfortunately, they did not provide a direct measure of the number of co-planar clusters. Recently, Tavares *et al.* [24], incorporated the dynamic effects in a spring element model using a random distribution of fibres.

The dynamic Stress Concentration Factor (*SCF*) with a plastic matrix in a non-hybrid composite was on average 43.2% higher, whereas it was 83.2% higher with an elastic matrix. Even though the dynamic effects caused an earlier formation of larger clusters, the number of co-planar clusters and the fibre break density did not significantly improve compared to the static model when an elasto-plastic matrix was considered. However, the authors did not study the influence the dynamic effects have on the hybrid composites. Therefore, the role of the dynamic phenomenon on the fibre tensile failure and cluster development of hybrid composites remains unexplored. Moreover, if the dynamic *SCF* is smaller in hybrid composites than in non-hybrids, hybrid effects may occur [18], but the importance of this has not yet been clarified.

Another common assumption in models is to neglect the thermal residual stresses resulting from the manufacturing process, which appear because of the different thermal expansion coefficient of the constituents. Different authors have demonstrated that the thermal residual stresses are secondary, since they can only account for up to 10% of the hybrid effects [17, 37, 38]. Nonetheless, their influence on cluster development has yet to be studied.

In this work, a progressive failure model [3, 4, 36], including thermal residual stresses and dynamic effects, is formulated. Their influence on the tensile failure process of hybrid composite materials is then investigated. The paper is organized as follows: firstly, the progressive failure model, including dynamic effects and thermal residual stresses, is presented. After that, some hybrid materials are simulated under fibre tensile loading to assess their influence and finally some conclusions are drawn.

2. Modelling approach

In this section the modelling strategy of this work is presented. Firstly, an analytical equation to determine thermal residual stresses for each fibre population derived from the manufacturing process is developed. Secondly, a progressive failure model [3, 4] is reviewed and modified by including thermal residual stresses and dynamic effects. To take the dynamic effects into account, a simple approach is considered based on Bullegas' work [35]. After a fibre fails, a dynamic iteration is performed in which the static *SCF* caused by the new failures is increased by a given dynamic factor. If at the end of the iteration no new failures occur, then the *SCF* values are reverted into the static conditions.

2.1. Analytical determination of thermal residual stresses

To determine the thermal residual stresses in a hybrid composite, two main hypothesis are applied following the approach in Prussak *et al.* [39]. Firstly, the force equilibrium in the fibre direction should lead to the summary of the force of all constituents (each fibre population and matrix) equal to zero, thus leading to

$$V_{\mathrm{f1}}\sigma^{\mathrm{r}}_{\mathrm{f1}} + V_{\mathrm{f2}}\sigma^{\mathrm{r}}_{\mathrm{f2}} + V_{\mathrm{m}}\sigma^{\mathrm{r}}_{\mathrm{m}} = 0 \tag{1}$$

Secondly, both fibre populations and matrix should have the same strain (including mechanical and thermal), thus

$$\frac{\sigma^{\mathrm{r}}_{\mathrm{f1}}}{E_{\mathrm{f1}}} + \alpha_{\mathrm{f1}}\left(T - T_{\mathrm{r}}\right) = \frac{\sigma^{\mathrm{r}}_{\mathrm{f2}}}{E_{\mathrm{f2}}} + \alpha_{\mathrm{f2}}\left(T - T_{\mathrm{r}}\right) = \frac{\sigma^{\mathrm{r}}_{\mathrm{m}}}{E_{\mathrm{m}}} + \alpha_{\mathrm{m}}\left(T - T_{\mathrm{r}}\right) \tag{2}$$

where V_{f1}, V_{f2}, V_{m} are the volume fractions ($V_{\mathrm{f1}} + V_{\mathrm{f2}} + V_{\mathrm{m}} = 1$), $\sigma^{\mathrm{r}}_{\mathrm{f1}}$, $\sigma^{\mathrm{r}}_{\mathrm{f2}}$, $\sigma^{\mathrm{r}}_{\mathrm{m}}$ are the longitudinal residual stresses, E_{f1}, E_{f2} and E_{m} are the Young's modulus whilst, α_{f1}, α_{f2} and α_{m} are the coefficient of thermal expansion, where sub-indices f1, f2 and m refer to fibre populations 1 and 2, and the matrix, respectively, whereas T is the test temperature and T_{r} is the stress-free reference temperature (usually the cure temperature). By mixing Eq. (1) and (2), the residual stresses become

$$\begin{aligned}
\sigma^{\mathrm{r}}_{\mathrm{f1}} &= E_{\mathrm{f1}}\frac{V_{\mathrm{f2}}E_{\mathrm{f2}}\left(\alpha_{\mathrm{f2}} - \alpha_{\mathrm{f1}}\right) + V_{\mathrm{m}}E_{\mathrm{m}}\left(\alpha_{\mathrm{m}} - \alpha_{\mathrm{f1}}\right)}{E_{\mathrm{f1}}V_{\mathrm{f1}} + E_{\mathrm{f2}}V_{\mathrm{f2}} + E_{m}V_{m}}\left(T - T_{\mathrm{r}}\right)\\
\sigma^{\mathrm{r}}_{\mathrm{f2}} &= E_{\mathrm{f2}}\frac{V_{\mathrm{f1}}E_{\mathrm{f1}}\left(\alpha_{\mathrm{f1}} - \alpha_{\mathrm{f2}}\right) + V_{\mathrm{m}}E_{\mathrm{m}}\left(\alpha_{\mathrm{m}} - \alpha_{\mathrm{f2}}\right)}{E_{\mathrm{f1}}V_{\mathrm{f1}} + E_{\mathrm{f2}}V_{\mathrm{f2}} + E_{m}V_{m}}\left(T - T_{\mathrm{r}}\right)\\
\sigma^{\mathrm{r}}_{\mathrm{m}} &= E_{\mathrm{m}}\frac{V_{\mathrm{f1}}E_{\mathrm{f1}}\left(\alpha_{\mathrm{f1}} - \alpha_{\mathrm{m}}\right) + V_{\mathrm{f2}}E_{\mathrm{f2}}\left(\alpha_{\mathrm{f2}} - \alpha_{\mathrm{m}}\right)}{E_{\mathrm{f1}}V_{\mathrm{f1}} + E_{\mathrm{f2}}V_{\mathrm{f2}} + E_{m}V_{m}}\left(T - T_{\mathrm{r}}\right)
\end{aligned} \tag{3}$$

while the residual strains can be determined with $\varepsilon^{\mathrm{r}}_{\mathrm{f1}} = \sigma^{\mathrm{r}}_{\mathrm{f1}}/E_{\mathrm{f1}}$, $\varepsilon^{\mathrm{r}}_{\mathrm{f2}} = \sigma^{\mathrm{r}}_{\mathrm{f2}}/E_{\mathrm{f2}}$ and $\varepsilon^{\mathrm{r}}_{\mathrm{m}} = \sigma^{\mathrm{r}}_{\mathrm{m}}/E_{\mathrm{m}}$. Note that for a non-hybrid composite the same equations can be applied by simply setting the quantities of one of the fibre populations equal to zero and thus leading to the same equations shown elsewhere as [40, 41].

2.2. Progressive Failure Model

The Progressive Failure Model (PFM) [3, 4, 36] is based on the chain of bundles approach and consists of a Representative Volume Element (RVE) of width a, height b and length L which contains a random distribution of fibres of a given radius. The fibres are divided into elements of length l along their longitudinal direction. For each element a different strength is assigned according to a statistical distribution. This leads to a domain of parallel tensile springs divided into planes in series. Each fibre is denoted with the sub-index $q \in \left[1, ..., N_q\right]$, which determines the position along the X and Y axes, while each plane is denoted with the sub-index $p \in \left[1, ..., N_p\right]$, which determines the position along the Z axis, where N_q and N_p are the number of fibres and planes respectively, see Fig. 1. When an element fails, the stress redistribution around the break is simulated by applying damage along the ineffective length of the broken fibre and stress concentration onto the neighbouring intact fibre elements. This approach allows fibre clustering and the stiffness loss of composite materials to be captured in a more computationally efficient way than other more sophisticated models [4, 36].

2.2.1. Constitutive equation

The constitutive equation which relates the element stress, $\sigma_{p,q}$, and the strain, ε_p, taking into account the residual strain now becomes

$$\sigma_{p,q} = \frac{SCF_{p,q}}{\Omega_p} E_q \left(1 - D_{p,q}\right)\left(\varepsilon_p + \varepsilon_q^{\mathrm{r}}\right) \tag{4}$$

where $SCF_{p,q}$ is the stress concentration factor (*SCF*) of element p, q, E_q is the Young's modulus of fibre q, $D_{p,q}$ is the damage state variable which is equal to 1 for broken elements, equal to 0 for intact elements and in between for elements in any stress recovery, ε_p is the mechanical strain of the plane (which is assumed to be the same for all elements of plane p), $\varepsilon_q^{\mathrm{r}}$ is the fibre's thermal residual strain determined with Eq. (3) and Ω_p is a stress ratio which enforces load equilibrium at each plane.

Calculating Ω_p and ε_p depends on a load equilibrium condition, whereas calculating $D_{p,q}$ and $SCF_{p,q}$ depends solely on an analytical model that is entered into the PFM. In theory, any model can be applied to predict both of them. Nonetheless, the models used should be consistent between them to obtain reliable results [36].

To take into account the dynamic effects, it is assumed here that the dynamic effects act by increasing the static *SCF* by a magnification factor, as has been proposed in other work [35]. Thus, after a fibre element fails, a dynamic iteration is performed and the static *SCF*s caused by the new failures are increased by a given factor. If at the end of the iteration no new failures occur, then the *SCF*s are reverted into the static values.

Therefore the dynamic effects are included in the calculation of the *SCF*. In the following, the remaining modelling equations and model process are explained.

2.2.2. Load equilibrium

Because the amount of damage may be different at each plane, each plane has its own mechanical strain, ε_p. Thus, ε_p is evaluated according to the stiffness of the RVE, the current strain applied at infinity, ε^0, and the residual strains. To do so, first the stiffness of each element, $k_{p,q}$, is calculated by Hooke's law with

$$k_{p,q} = E_q \left(1 - D_{p,q}\right) \frac{A_q}{l} \tag{5}$$

where A_q is the fibre's cross-sectional area. The stiffness of each plane, k_p, and the stiffness of each plane for fibre populations 1 and 2 (f1 and f2), are then computed by assuming all elements and the matrix in the plane work in parallel

$$k_{p_1} = \sum_{q \in \mathrm{f1}}^{N_q} k_{p,q} \qquad k_{p_2} = \sum_{q \in \mathrm{f2}}^{N_q} k_{p,q} \qquad k_p = k_{p_1} + k_{p_2} + k_{\mathrm{m}} \tag{6}$$

where k_{m} is the matrix stiffness, $k_{\mathrm{m}} = E_{\mathrm{m}} A_{\mathrm{m}}/l$, E_{m} is the matrix Young's modulus and A_{m} the matrix's cross-sectional area, $A_{\mathrm{m}} = a\ b - \sum_{q=1}^{N_q} A_q$. Next, the total stiffness of the system is computed by assuming all planes work in series

$$K = \left(\sum_{p=1}^{N_p} \frac{1}{k_p} \right)^{-1} \tag{7}$$

Finally, ε_p can be obtained by load equilibrium, as the total mechanical and thermal force of each plane, $F_p = k_p \varepsilon_p l + k_{p_1} \varepsilon_{\mathrm{f1}}^{\mathrm{r}} l + k_{p_2} \varepsilon_{\mathrm{f2}}^{\mathrm{r}} l + k_{\mathrm{m}} \varepsilon_{\mathrm{m}}^{\mathrm{r}} l$, must be equal to the force applied, $F = K \varepsilon^0 L$, leading to

$$\varepsilon_p = \frac{K \varepsilon^0}{k_p} \frac{L}{l} - \frac{k_{p_1} \varepsilon_{\mathrm{f1}}^{\mathrm{r}} + k_{p_2} \varepsilon_{\mathrm{f2}}^{\mathrm{r}} + k_{\mathrm{m}} \varepsilon_{\mathrm{m}}^{\mathrm{r}}}{k_p} \tag{8}$$

where ε^0 is the applied strain and $\varepsilon_{\mathrm{f1}}^{\mathrm{r}}$, $\varepsilon_{\mathrm{f2}}^{\mathrm{r}}$ and $\varepsilon_{\mathrm{m}}^{\mathrm{r}}$ are the residual strains of fibre populations 1 and 2, and the matrix, respectively, determined with Eq. (3).

To maintain local load equilibrium, the aggregation of the loads of the fibres and the matrix at each plane, p, must be equal to the load of the plane F_p. This condition allows the stress ratio Ω_p to be obtained with

$$F_p = \sum_{q=1}^{N_q} \left(\frac{SCF_{p,q}}{\Omega_p} E_q \left(1 - D_{p,q}\right) \left(\varepsilon_p + \varepsilon_q^{\mathrm{r}}\right) A_q \right) + \left(\varepsilon_p + \varepsilon_m^{\mathrm{r}}\right) E_{\mathrm{m}} A_{\mathrm{m}}$$
$$\Omega_p = \frac{\sum_{q=1}^{N_q} SCF_{p,q} E_q \left(1 - D_{p,q}\right) \left(\varepsilon_p + \varepsilon_q^{\mathrm{r}}\right) A_q}{\left(k_p \varepsilon_p + k_{p_1} \varepsilon_{\mathrm{f1}}^{\mathrm{r}} + k_{p_2} \varepsilon_{\mathrm{f2}}^{\mathrm{r}} - k_{\mathrm{m}} \varepsilon_p\right) l} \tag{9}$$

2.2.3. Ineffective length and damage

The ineffective length of broken fibres depends mainly on the matrix behaviour, which can be elastic or plastic, as debonding is omitted here [4, 36]. The matrix behaviour is a key factor in the modelling predictions as it changes the ineffective length and the magnitude of the *SCF* over the intact fibres [4, 12, 36, 42].

For a plastic matrix, the model is modified as to include the residual strain. Therefore, the ineffective length corresponds to a modified Kelly-Tyson shear-lag model [43]. The ineffective length includes a scaling factor, H, which scales the ineffective length according to the cluster size [44]. This cluster is calculated assuming that two broken fibre elements belong to the same cluster (c), if the distance between the centres of both fibres is below four times the smallest fibre radius and both elements are on the same plane p [4, 36]. Each cluster of plane p is represented with the sub-index p, c, with $c \in \left[1, ..., N_p^c\right]$ where N_p^c is the total number of clusters on plane p. Thus, the ineffective length of a broken fibre element in cluster p, c is

$$L_{p,q}^{\mathrm{in}} = \frac{R_q E_q}{2\tau_q} H_{p,c} \left(\varepsilon_p + \varepsilon_q^{\mathrm{r}}\right) = \frac{n_{p,c} \pi R_q^2 E_q}{C_{p,c} \tau_q} \left(\varepsilon_p + \varepsilon_q^{\mathrm{r}}\right) \tag{10}$$

where τ_q is the matrix shear yield stress, R_q is the fibre radius, $C_{p,c} = 4s\sqrt{n_{p,c}}$, and where $n_{p,c}$ is the number of broken fibres on cluster p, c and s is the overall mean distance between fibre centres, $s = \left[\left(R_{\mathrm{f1}} V_{\mathrm{f1}} + R_{\mathrm{f2}} V_{\mathrm{f2}}\right) / V_{\mathrm{f}}\right] \sqrt{\pi / V_{\mathrm{f}}}$, where R_{f1} and R_{f2} are the fibre radius of fibre populations 1 and 2 respectively and V_{f} is the overall fibre volume fraction, $V_{\mathrm{f}} = V_{\mathrm{f1}} + V_{\mathrm{f2}}$. The damage of element p, q due to each break in the fibre q at each plane i is computed following the ineffective length curve as

$$D_{p,q} = \begin{cases} \max\left(\dfrac{L_{i,q}^{\mathrm{in}} - |i - p|\, l}{L_{i,q}^{\mathrm{in}}}\right) & \forall i : \left(D_{i,q} = 1\right) \cup \left(|i - p|\, l < L_{i,q}^{\mathrm{in}}\right) \\ 0 & \text{otherwise.} \end{cases} \tag{11}$$

If an elastic matrix is assumed, then the ineffective length is based on Cox's shear-lag model [45, 46]. For this scenario, the ineffective length depends neither on the residual strain nor on the mechanical strain [36], and is given by [4]

$$L^{\text{in}}_{p,q} = H_{p,c}\sqrt{\frac{E_q R_q}{2G_{\text{m}}}\left(s - 2\frac{R_{\text{f1}}V_{\text{f1}} + R_{\text{f2}}V_{\text{f2}}}{V_{\text{f}}}\right)}\ln\left(\frac{1}{1-\zeta}\right) \tag{12}$$

where G_{m} is the matrix shear modulus. It is worth mentioning that this length corresponds to a recovery of ζ percent of the nominal fibre stress (in this work $\zeta = 99.9\%$ of the nominal fibre stress [4, 36]). The damage is then computed with

$$D_{p,q} = \begin{cases} \max\left(\exp\left(-\frac{|i-p|\,l}{H_{p,c}}\sqrt{\frac{2G_{\text{m}}}{E_q R_q\left(s - 2\frac{R_{\text{f1}}V_{\text{f1}} + R_{\text{f2}}V_{\text{f2}}}{V_{\text{f}}}\right)}}\right)\right) & \forall i : \left(D_{i,q} = 1\right) \cup \left(|i-p|\,l < L^{\text{in}}_{i,q}\right) \\ 0 & \text{otherwise.} \end{cases} \tag{13}$$

Nonetheless, as was demonstrated in Guerrero *et al.* [4], the use of an elastic matrix may lead to inaccurate results when modelling hybrid composites. Consequently, in this work the matrix is assumed to be plastic and the ineffective length and damage are calculated with Eqs. (10) and (11).

2.2.4. Stress concentration factor and dynamic effects

To predict the static *SCF* around breaks, different models can be found in the literature [5, 44, 47, 48]. In this work, the proposed model, which has been used in previous studies and is based on the work of St-Pierre *et al.* [44], is applied [4]. The model is very powerful as it can predict the static *SCF* around a cluster i, c of broken fibres located on the same plane, taking into account the cluster size, RVE size, volume fractions, fibre radius and elastic properties of each fibre population. Furthermore, it can be calibrated to take into account different effects not present in the model [4].

The complex dynamic effects are simulated in this work in a simple and efficient way by adapting the approach proposed in Bullegas [35]. When a new element fails, a dynamic iteration is started. The static increment of *SCF* produced by the cluster i, c, to which the broken element belongs to, is multiplied by a factor larger than 1, M_{d}. This factor is only applied to the *SCF* produced by clusters i, c with new breaks, while it is equal to 1 for all other clusters i, c with no new broken elements. If no new elements fail at the end of the dynamic iteration, then all factors are set equal to 1 and the model reverts to static conditions. However, if new elements fail, then a new dynamic iteration is started. Hence, the static SCF caused by any cluster i, c with new broken fibres is multiplied by M_{d}.

It should be noted that the proposed approach does not allow the entire dynamic process to be captured, as unlike other models [24], the time variable is omitted. Within this approach, only the instant of time at which the maximum dynamic effect is produced is considered. Notwithstanding, that is the only time instant of interest as any new failures will occur when the SCF is maximum. Therefore, this method allows for a more efficient simulation process. In addition, it is assumed that the behaviour is quasi-static, since dynamic effects only occur as a result of new breaks and not to the applied load. Further to this, it is considered that the dynamic factor, M_{d}, is independent of the number of simultaneous breaks that occur in the cluster i, c, in accordance with the results of Tavares *et al.* [24].

The static increment of SCF for an intact element p, q due to cluster i, c is given by $\Delta SCF = \delta \cdot \lambda$, where δ and λ are two functions [4]. The function δ is related to the in-plane distance $\left(r_{q-c}\right)$ between the geometrical centre of coordinates of cluster i, c and intact element p, q, while λ is related to the plane position along the ineffective length. Because an intact element can receive SCF from broken fibres from the same or other population, and each cluster can contain broken fibres of each population, four combinations for δ occur

$$\begin{aligned} \delta_{11_{(q-c)}} &= I_{11_{i,c}} \left(\frac{R_{i,c}}{r_{q-c}}\right)^{\alpha} \qquad & \delta_{22_{(q-c)}} &= I_{22_{i,c}} \left(\frac{R_{i,c}}{r_{q-c}}\right)^{\alpha} \\ \delta_{12_{(q-c)}} &= I_{12_{i,c}} \left(\frac{R_{i,c}}{r_{q-c}}\right)^{\alpha} \qquad & \delta_{21_{(q-c)}} &= I_{21_{i,c}} \left(\frac{R_{i,c}}{r_{q-c}}\right)^{\alpha} \end{aligned} \tag{14}$$

Similarly, each cluster i, c has two ineffective lengths, the ineffective length of broken elements of type 1, $L^{\mathrm{in}}_{1_{i,c}}$, and that of broken elements of type 2, $L^{\mathrm{in}}_{2_{i,c}}$. Therefore, two combinations for λ occur

$$\begin{aligned} \lambda_{1_{(p-i)}} &= \begin{cases} \dfrac{L^{\mathrm{in}}_{1_{i,c}} - l\,|i-p|}{L^{\mathrm{in}}_{1_{i,c}}} & \forall (i,c) : \; l\,|i-p| < L^{\mathrm{in}}_{1_{i,c}} \quad \text{Plastic matrix} \\ \exp\left(-\dfrac{|i-p|\, l C_{i,c}}{2\pi n_{i,c} R_{\mathrm{f1}}^2} \sqrt{\dfrac{2 G_{\mathrm{m}} R_{\mathrm{f1}}}{E_{\mathrm{f1}}\left(s - 2\dfrac{R_{\mathrm{f1}} V_{\mathrm{f1}} + R_{\mathrm{f2}} V_{\mathrm{f2}}}{V_{\mathrm{f}}}\right)}} \right) & \forall (i,c) : \; l\,|i-p| < L^{\mathrm{in}}_{1_{i,c}} \quad \text{Elastic matrix} \end{cases} \\ \lambda_{2_{(p-i)}} &= \begin{cases} \dfrac{L^{\mathrm{in}}_{2_{i,c}} - l\,|i-p|}{L^{\mathrm{in}}_{2_{i,c}}} & \forall (i,c) : \; l\,|i-p| < L^{\mathrm{in}}_{2_{i,c}} \quad \text{Plastic matrix} \\ \exp\left(-\dfrac{|i-p|\, l C_{i,c}}{2\pi n_{i,c} R_{\mathrm{f2}}^2} \sqrt{\dfrac{2 G_{\mathrm{m}} R_{\mathrm{f2}}}{E_{\mathrm{f2}}\left(s - 2\dfrac{R_{\mathrm{f1}} V_{\mathrm{f1}} + R_{\mathrm{f2}} V_{\mathrm{f2}}}{V_{\mathrm{f}}}\right)}} \right) & \forall (i,c) : \; l\,|i-p| < L^{\mathrm{in}}_{2_{i,c}} \quad \text{Elastic matrix} \end{cases} \end{aligned} \tag{15}$$

where $\delta_{11_{(q-c)}}$ and $\delta_{22_{(q-c)}}$ correspond to the static increment of *SCF* that an intact element from fibre populations 1 and 2, respectively, receives due to broken fibres of its own type in cluster i, c, while $\delta_{12_{(p-i)}}$ and $\delta_{21_{(p-i)}}$ are the static increments of *SCF* that an element of fibre populations 1 and 2, respectively, receives due to broken fibres of a different type in cluster i, c. $\lambda_{1_{(p-i)}}$ is the evolution of $\delta_{11_{(q-c)}}$ and $\delta_{21_{(q-c)}}$ along $L^{\text{in}}_{1_{i,c}}$, while $\lambda_{2_{(p-i)}}$ is the evolution of $\delta_{22_{(q-c)}}$ and $\delta_{12_{(q-c)}}$ along $L^{\text{in}}_{2_{i,c}}$. $R_{i,c}$ is the equivalent radius of the cluster, $\pi R^2_{i,c} = n_{i,c} S^2_{i,c}$, $S_{i,c}$ is the average fibre spacing of the cluster, $S_{i,c} = \left[\left(n_{1_{i,c}} R_{\text{f1}} + n_{2_{i,c}} R_{\text{f2}}\right)/n_{i,c}\right] \sqrt{\pi/V_{\text{f}}}$, $n_{1_{i,c}}$ and $n_{2_{i,c}}$ are the number of broken fibres in populations 1 and 2, respectively, in cluster i, c, and $n_{i,c} = n_{1_{i,c}} + n_{2_{i,c}}$. The exponent α is an input parameter which governs the maximum value of *SCF* and the shape of the curve. Its value can be adopted as $\alpha = 2$ for a plastic matrix or $\alpha = 3.8$ for an elastic matrix [4, 36, 44]. As this work assumes a plastic matrix, $\alpha = 2$ will be used.

The terms I are constants which differ for each cluster i, c and are given by

$$
\begin{aligned}
I_{11_{i,c}} &= \begin{cases} \dfrac{n_{1_{i,c}} R^2_{\text{f1}} R^2_{\text{f2}}}{2R^2_{i,c} \ln\left(R_{\text{t}}/R_{i,c}\right)\left(R^2_{\text{f1}} V_{\text{f2}} + R^2_{\text{f2}} V_{\text{f1}}\right)} & \text{for } \alpha = 2 \\ \dfrac{n_{1_{i,c}} R^2_{\text{f1}} R^2_{\text{f2}} R^{-\alpha}_{i,c} (\alpha - 2)}{2\left(R^{2-\alpha}_{i,c} - R^{2-\alpha}_{\text{t}}\right)\left(R^2_{\text{f1}} V_{\text{f2}} + R^2_{\text{f2}} V_{\text{f1}}\right)} & \text{otherwise,} \end{cases} \\
I_{21_{i,c}} &= \begin{cases} \dfrac{E_{\text{f1}} n_{1_{i,c}} R^4_{\text{f1}}}{2E_{\text{f2}} R^2_{i,c} \ln\left(R_{\text{t}}/R_{i,c}\right)\left(R^2_{\text{f1}} V_{\text{f2}} + R^2_{\text{f2}} V_{\text{f1}}\right)} & \text{for } \alpha = 2 \\ \dfrac{E_{\text{f1}} n_{1_{i,c}} R^4_{\text{f1}} R^{-\alpha}_{i,c} (\alpha - 2)}{2E_{\text{f2}}\left(R^{2-\alpha}_{i,c} - R^{2-\alpha}_{\text{t}}\right)\left(R^2_{\text{f1}} V_{\text{f2}} + R^2_{\text{f2}} V_{\text{f1}}\right)} & \text{otherwise,} \end{cases} \\
I_{22_{i,c}} &= \begin{cases} \dfrac{n_{2_{i,c}} R^2_{\text{f1}} R^2_{\text{f2}}}{2R^2_{i,c} \ln\left(R_{\text{t}}/R_{i,c}\right)\left(R^2_{\text{f1}} V_{\text{f2}} + R^2_{\text{f2}} V_{\text{f1}}\right)} & \text{for } \alpha = 2 \\ \dfrac{n_{2_{i,c}} R^2_{\text{f1}} R^2_{\text{f2}} R^{-\alpha}_{i,c} (\alpha - 2)}{2\left(R^{2-\alpha}_{i,c} - R^{2-\alpha}_{\text{t}}\right)\left(R^2_{\text{f1}} V_{\text{f2}} + R^2_{\text{f2}} V_{\text{f1}}\right)} & \text{otherwise,} \end{cases} \\
I_{12_{i,c}} &= \begin{cases} \dfrac{E_{\text{f2}} n_{2_{i,c}} R^4_{\text{f2}}}{2E_{\text{f1}} R^2_{i,c} \ln\left(R_{\text{t}}/R_{i,c}\right)\left(R^2_{\text{f1}} V_{\text{f2}} + R^2_{\text{f2}} V_{\text{f1}}\right)} & \text{for } \alpha = 2 \\ \dfrac{E_{\text{f2}} n_{2_{i,c}} R^4_{\text{f2}} R^{-\alpha}_{i,c} (\alpha - 2)}{2E_{\text{f1}}\left(R^{2-\alpha}_{i,c} - R^{2-\alpha}_{\text{t}}\right)\left(R^2_{\text{f1}} V_{\text{f2}} + R^2_{\text{f2}} V_{\text{f1}}\right)} & \text{otherwise,} \end{cases}
\end{aligned}
\tag{16}
$$

where R_{t} is the RVE equivalent radius, $R_{\text{t}} = \sqrt{(a \cdot b)/\pi}$.

To take into account the interaction between different clusters, a superposition rule is considered. The total *SCF* for an intact fibre element is obtained by the linear superposition of the *SCF* it receives from all clusters i, c. Nonetheless, to achieve stress continuity between elements inside any ineffective length (elements where $0 < D_{p,q} < 1$) that are not affected by the SCF, and subsequent intact elements ($D_{p,q} = 0$), which can be overloaded by the SCF, the SCF of an element is limited according to shear-lag transfer [3, 4, 36]. Thus, the total SCF of an intact element p, q is

$$SCF_{p,q} = \begin{cases} \min\left(SCF^0_{p,q}, SCF^{\mathrm{L}}_{p,q}\right) & \forall p, q : D_{p,q} = 0 \\ 1 & \text{otherwise,} \end{cases} \tag{17}$$

where $SCF^0_{p,q}$ is the SCF predicted by the linear superposition of the contribution of all clusters, taking into account the dynamic effect using the previous δ and λ functions with

$$\begin{aligned} SCF^0_{p,q} &= 1 + \sum_{i=1}^{N_p} \sum_{c=1}^{N_i^c} M_{1_{i,c}} \delta_{11_{(q-c)}} \lambda_{1_{(p-i)}} + M_{2_{i,c}} \delta_{12_{(q-c)}} \lambda_{2_{(p-i)}} \quad \forall i, c : n_{i,c} > 0 \quad \& \quad q \in \mathrm{f1} \\ SCF^0_{p,q} &= 1 + \sum_{i=1}^{N_p} \sum_{c=1}^{N_i^c} M_{2_{i,c}} \delta_{22_{(q-c)}} \lambda_{2_{(p-i)}} + M_{1_{i,c}} \delta_{21_{(q-c)}} \lambda_{1_{(p-i)}} \quad \forall i, c : n_{i,c} > 0 \quad \& \quad q \in \mathrm{f2} \end{aligned} \tag{18}$$

where f1 and f2 are fibre populations 1 and 2, respectively, while $M_{1_{i,c}}$ and $M_{2_{i,c}}$ are the dynamic factors caused by new breaks in populations 1 and 2, respectively, in cluster i, c. As detailed at the beginning of this subsection, these factors are equal to 1 for any cluster i, c in which no new breaks occurred. Nevertheless, if any new broken elements of type 1 appear in cluster i, c, then $M_{1_{i,c}} = M_{\mathrm{d}}$. Similarly, if new broken elements of type 2 appear then $M_{2_{i,c}} = M_{\mathrm{d}}$. Therefore, many different combinations may occur because, an intact element may receive dynamic SCF from the two populations in the cluster or from only one of them, or it may receive dynamic SCF from one cluster and static SCF from another different cluster. Finally, $SCF^{\mathrm{L}}_{p,q}$ is the SCF limitation for broken fibre q, and it is calculated as in previous work [3, 4, 36]:

$$SCF^{\mathrm{L}}_{p,q} = \min\left(\frac{1}{L^{\mathrm{in}}_{i,q}} |i - p| \, l\right) \quad \forall i : D_{i,q} = 1 \tag{19}$$

2.2.5. Numerical implementation

A uniaxial strain controlled simulation is performed along the fibre longitudinal direction by slowly increasing the applied strain, ε^0. In this way, a progressive and stable damage process can be simulated. A step-by-step implementation of the model is shown in Algorithm 1. Before starting the simulation, the strength of each element is generated following a given statistical distribution, and if they are to be considered the thermal residual stresses are estimated, as given in lines 1-2 of the algorithm. After that, a new loading step is started by applying a uniaxial strain, see line 3. At each new iteration, y, of the model, the objective is to compute the stress of each element by following the procedure shown in lines 5-11 of the algorithm. Next, the stresses are compared with the strengths, as given in line 12. At this point two possibilities may arise: 1) new elements fail and, consequently, lines 13-16 of the algorithm are applied, or 2) no new elements fail, and thus lines 18-20 are employed. If no new elements fail, then the algorithm applies static conditions, i.e. $M_{1_{p,c}} = 1$ and $M_{2_{p,c}} = 1$ for all clusters p, c. Then a new static step, is started by increasing the applied strain. However, if new elements fail, a damage factor equal to 1 is assigned to all new broken elements. Then, all clusters p, c are determined. For the clusters p, c with new breaks of type 1, $M_{1_{p,c}} = M_{\mathrm{d}}$. Similarly for the clusters p, c with new breaks of type 2, $M_{2_{p,c}} = M_{\mathrm{d}}$ is assigned. For all clusters with no new breaks $M_{1_{p,c}} = 1$ and $M_{2_{p,c}} = 1$. The algorithm then starts a dynamic iteration by repeating the whole process. The process shown continues until either all elements in a plane are broken, or the average fibre stress of the HE fibre population has decreased in a single step, t, by a pre-defined percentage of the maximum load value. A small decrease of 10%, is enough to capture the final failure of the material and also allows computational time to be reduced.

3. Methodology

To study the influence both thermal residual stresses and dynamic phenomenon have on the tensile failure of hybrid composites, different materials are simulated using the PFM. To quantify their importance separately, the tensile behaviour is simulated three times: a) under static conditions (i.e. $M_{\mathrm{d}} = 1$) and without thermal residual stresses, b) under static conditions with thermal residual stresses, and c) under dynamic conditions (i.e. $M_{\mathrm{d}} \neq 1$) and without thermal residual stresses. For the dynamic cases, the value of M_{d} is varied between 1.25, 1.43, 1.6 and 2. These values are taken from the literature: 1.43 corresponds to the average result given in Tavares *et al.* [24] using a plastic matrix, while 1.6 corresponds to the result of Hedgepeth [20] and 2 is a theoretical maximum factor for a spring-mass system without damping [35]. Likewise for the thermal residual stresses, two extreme values (a lower bound and an upper bound) for the coefficient of thermal expansion of both LE and HE fibres in the materials are used to observe their impact. To calculate them, the test temperature is assumed to be $T = 25°C$, whereas the stress-free temperature is $T_\mathrm{r} = 150°C$.

To observe the impact of the dynamic phenomenon and thermal residual stresses with diverse material properties, different intrayarn hybrid unidirectional composites are simulated by combining various carbon and glass fibres. These hybrids correspond to X5-T300 (Carbon-Carbon), T300-Eglass (Carbon-Glass) and X5-Eglass (Carbon-Glass). These material combinations are interesting as, in all cases, the failure strain of both fibre populations should be fairly well apart, and all LE fibres have a relatively small Weibull modulus which is known to be positive for the hybrid effect [9–11]. In all cases, the matrix is always Epoxy with properties $E_\mathrm{m} = 3760$ MPa, $\tau_q = 50$ MPa and $\alpha_\mathrm{m} = 58 \cdot 10^{-6}$ $°C^{-1}$ [11, 49]. The corresponding properties of each fibre can be seen in Table 1.

A modified version of Melro's random fibre generator [11, 50] is used to create an RVE of width, thickness and length of (respectively) $75 \times 75 \times 300$ times the largest fibre radius on the RVE. The element length, l, is equal to the smallest fibre diameter in the RVE. The overall volume fraction (V_f) is always 60%. However, because the hybrid volume fraction (HVF) is known to have a considerable impact on the tensile response of hybrid composites [4, 8, 10, 11, 51], each hybrid is simulated with an HVF of 10, 20, 30, 40, 50 and 75%. Here, the HVF is the percentage of LE fibre volume fraction (V_LE) over the total volume fraction (V_f), $HVF = (V_\mathrm{LE}/V_\mathrm{f})$. In addition, a non-hybrid composite of each fibre type is also simulated.

As in other work [3–5, 12, 36], the strength of each element in the RVE is given by a Weibull distribution [52]. To generate them, a random number between 0 and 1 is assigned for each element, $P_{p,q}$. The strength of the element, $\sigma^\mathrm{u}_{p,q}$, is then computed according to the Weibull distribution function with $P_{p,q} = 1 - \exp\left(-(l/L_0)\left(\sigma^\mathrm{u}_{p,q}/\sigma_0\right)^m\right)$, using the corresponding Weibull properties, σ_0, m, L_0 of the fibre given in Table 1. Because of the random nature of the fibre strength and the random position of the fibres, 8 runs are performed for each case in study. For each run, a new RVE and new element strengths are generated. However, the same RVEs and fibre strengths are used for the static, dynamic and thermal residual stress cases to allow for a fair comparison between them.

To compare the results between simulations, different metrics are used [4]. Firstly, the failure strength, σ^ult, which corresponds to the maximum stress reached by the material.

Secondly, the failure strain, $\varepsilon^{\mathrm{ult}}$, which corresponds to the strain at σ^{ult}. Thirdly, the yield stress (σ^{y}), which is defined as the knee point at a strain of 0.1% where the stress-strain curve deviates from the initial linear elastic region. And fourthly, the pseudo-ductile strain ($\varepsilon^{\mathrm{d}} = \varepsilon^{\mathrm{ult}} - \sigma^{\mathrm{ult}}/E_0$), where E_0 is the initial Young's modulus of the composite given by the rule of mixtures.

The fifth metric is the maximum cluster of broken fibres in the RVE, N^{c}, at failure. To track these clusters along the simulation, it is assumed that two broken elements belong to the same cluster if their distance between centres is smaller than 4 times the smallest fibre radius and the distance between break planes is less than 10 times the smallest fibre radius [4, 5, 9, 12, 36]. A cluster is assumed to be co-planar if the axial distance between all brake planes in the cluster is smaller than or equal to one element length, otherwise it is a diffuse cluster [5, 12]. It should be noted that, the maximum cluster size shown in the results is different from the cluster definition that was used in section 2.2.3 to calculate the *SCFs* and ineffective length. This was done to allow the damage evolution to be measured in the same way as it has been done in the literature.

It is worth mentioning that the RVE volumes used in this study, which are as small as $0.26 \times 0.26 \times 1.05$ mm and as large as $0.6 \times 0.6 \times 2.4$ mm, and contain as few as 1100 fibres and as many as 4500 fibres, are small compared to a real material specimen. Due to the size effects present in composite materials, the strengths obtained, σ^{ult}, may not be representative of real composites. Moreover, the Weibull distribution used to calculate the fibre strengths is extrapolated to the element length, l, which is very small. This is known to cause an overprediction of the strength. Further discussion related to size effects and Weibull distribution issues can be found elsewhere [36, 42].

4. Results

In this section the influence both thermal residual stresses and dynamic effects have on the failure process and cluster development of broken fibres for the different hybrids simulated is analysed. All results correspond to the average of 8 runs.

4.1. Dynamic effects

Overall, the maximum cluster size, shown in Fig. 2 a)-c), increases with the dynamic factor. In general, this increase seems to be larger for the composites that are less damage tolerance, i.e. the non-hybrid composites and the hybrids with larger *HVF*. Nevertheless, the formation of co-planar clusters shown in Fig. 2 d)-f) presents a negligible variation for the dynamic factor.

The influence of the dynamic effects on the failure strain and ductile strain is shown in Fig. 3. Overall, there is a minor decrease in the failure strain when the dynamic factor is increased. For both the X5-Eglass and X5-T300 composites, shown in Fig. 3 b) and c), the decrease in failure strain is larger for the non-hybrid composites than it is for the hybrids. However, this does not occur with the T300-Eglass composite shown in Fig. 3 a), which presents a larger decrease of failure strain for the hybrid composites with $HVF = 10\%$ and $HVF = 20\%$ than it does for the non-hybrids when $M_\mathrm{d} = 2$. Regarding the ductile strain, similar trends are highlighted. In general, there is a minor decrease in the ductile strain when the dynamic factor is increased. This decrease is seen to be larger for the T300-Eglass hybrid composites with $HVF = 10\%$ and $HVF = 20\%$.

The failure stress and yield stress of the simulated composites is shown in Fig. 4. As with the failure strain, the failure strength also presents a small decrease when increasing the dynamic factor, although the decrease is mostly negligible. In regards to the yield stress, no changes at all are observed for the hybrid composites.

The tensile behaviour predicted for each composite is seen to be very different and to be heavily dependent on the *HVF*, as illustrated in Fig. 5. A large pseudo-ductile strain of 0.6-0.8% is predicted with the X5-T300 hybrid for an *HVF* of between 10-50%, whilst at larger *HVF*, brittle behaviours are obtained. An even larger pseudo-ductile strain of 1.25-1.5% can be observed for the X5-Eglass composite for an *HVF* of between 10-30%. For the last hybrid studied, T300-Eglass, a ductile strain of 0.6-0.8% for an *HVF* of between 10-20% is found. As has been discussed, the dynamic effects lead to a slightly earlier failure, but do not significantly change the tensile behaviour.

4.2. Thermal residual stresses

The influence thermal residual stresses have on the formation of clusters is shown in Fig. 6. Overall the thermal residual stresses do not have a significant impact on cluster formation. The maximum variation in cluster size can be seen for the X5-Eglass hybrid composite for $HVF = 30\%$, showing a change of 10 fibres compared to the case without thermal residual stresses. For the co-planar clusters, the variation is less than 1% for all composites.

The influence of thermal residual stresses on the failure and ductile strains is shown in Fig. 7. In some composites a minor variation of these two strains is seen when the residual stresses are considered. For the X5-T300 composite, the failure strain and ductile strain present a minor increase when $\alpha_{\mathrm{LE}} = 7 \cdot 10^{-6}$ $°C^{-1}$ and $\alpha_{\mathrm{HE}} = -7 \cdot 10^{-6}$ $°C^{-1}$ and a small decrease for the opposite combination. For the other two combinations of α_{LE} and α_{HE}, the results lie somewhere in between. The same trend is seen for the X5-Eglass and T300-Eglass composites. The ductile composites, corresponding to $HVF = 10 - 30\%$, experience an increase in failure strain and ductile strain when $\alpha_{\mathrm{LE}} = 7 \cdot 10^{-6}$ $°C^{-1}$ and $\alpha_{\mathrm{HE}} = 5 \cdot 10^{-6}$ $°C^{-1}$, and a decrease when $\alpha_{\mathrm{LE}} = -7 \cdot 10^{-6}$ $°C^{-1}$ and $\alpha_{\mathrm{HE}} = 10 \cdot 10^{-6}$ $°C^{-1}$.

In regards to the failure stress and yield stress shown in Fig. 8, a minor variation can also be observed with the thermal residual stresses. For the X5-T300 composite, the strength and yield stress are the largest when $\alpha_{\mathrm{LE}} = -7 \cdot 10^{-6}$ $°C^{-1}$ and $\alpha_{\mathrm{HE}} = 7 \cdot 10^{-6}$ $°C^{-1}$, while they are the smallest when $\alpha_{\mathrm{LE}} = 7 \cdot 10^{-6}$ $°C^{-1}$ and $\alpha_{\mathrm{HE}} = -7 \cdot 10^{-6}$ $°C^{-1}$. Similarly, for the X5-Eglass and T300-Eglass the maximum occurs when $\alpha_{\mathrm{LE}} = -7 \cdot 10^{-6}$ $°C^{-1}$ and $\alpha_{\mathrm{HE}} = 10 \cdot 10^{-6}$ $°C^{-1}$ and the minimum for the opposite combination. For the other combinations of coefficient of thermal expansion, the results lie between these.

The tensile behaviour obtained is not shown since it is qualitatively the same as that illustrated in Fig. 5.

5. Discussion

5.1. Influence of dynamic effects

As proved in Fig. 2, the maximum cluster size increases as the dynamic factor does. This can be easily understood. Since increasing the dynamic factor leads to higher *SCF*, the probability of creating larger clusters is also greater. These findings imply that the dynamic effects change the damage development of the materials, leading to an earlier formation of larger clusters in the dynamic model than in the static model. This emphasizes the importance of including dynamic effects. Considering them should, in theory, lead to a more realistic formation of clusters compared to experiments. Nevertheless, the formation of co-planar clusters is seen to be unaffected by the dynamic effects. Thus, increasing the dynamic factor does not increase the formation of co-planar clusters, as was supposed in the literature [5, 42]. This corresponds well to the recent findings of Tavares *et al.* [24]. Such outcomes suggest that, the underprediction of co-planar clusters seen in most of the models in the literature may not be related to the omission of dynamic effects. It should be noted that the formation of clusters depends on the specific RVE and fibre strengths of each run. In other words, owing to the variability of the results, some of the curves in Fig. 2 may intersect.

As evidenced in Fig. 3, a minor decrease in the failure strain and ductile strain occurs when considering dynamic effects. In some hybrid composites such as the X5-Eglass and X5-T300, the decrease in failure strain is larger for the non-hybrid composites than for the hybrids, which suggests the presence of a small positive hybrid effect caused by the dynamic effects. However, this does not occur with the T300-Eglass composite which presents a larger decrease of failure strain for the hybrid composites comprising a low *HVF*. These results suggest that, although the dynamic effects change the formation of clusters, they do not have any significant influence on the final failure or on the ductility of the composite. This is something that corresponds well to the findings of Tavares *et al.* [24] in non-hybrid composites using an elasto-plastic matrix.

A minor decrease in strength is also seen when considering the dynamic effects as illustrated in Fig. 4. The yield stress presents no changes at all due to the dynamic effects. This is because the yield stress depends mainly on the initiation of damage when the number of breaks is still small. At that point, the dynamic effects are not important.

The tensile behaviour predicted for each composite, shown in Fig. 5, proves that a ductile failure process can be achieved via fibre hybridization. A very large ductile strain between 1.25-1.5% is obtained with the X5-Eglass composite for an *HVF* between 10-30%. That large pseudo-ductile strain is possible thanks to the fact that the failure strain of the two fibres in the hybrid is well apart, and the failure process is continuous. In any case, it can be seen that the dynamic effects lead to a slightly earlier failure, but do not significantly change the tensile behaviour.

The results obtained show that the dynamic phenomenon has an effect on the formation of clusters, leading to larger clusters at smaller strains compared to the static model.

Nonetheless, final failure is not significantly altered, as the failure strain and strength are marginally smaller in the dynamic model. The tensile behaviour is also seen to be unaffected. This contradicts the general belief in the literature that the dynamic effects considerably influence final failure [5, 42]. Additionally, if the dynamic factor is smaller in the hybrid composites than that of the baseline non-hybrid composites, as the work of Xing *et al.* [18] suggests, hybrid effects should occur due to the dynamic phenomenon. However, the results presented by varying the dynamic factor, M_{d}, show a very reduced effect. Therefore, the contribution the dynamic phenomenon makes to the hybrid effect seems to be very small. These results have been obtained by using a plastic matrix approach. Using an elastic matrix should lead to the dynamic effects having a greater influence on final failure, as pointed in Tavares *et al.* [24]. Nonetheless, a plastic matrix should be a more realistic representation of the failure process [4]. Adding the dynamic effects should allow a more accurate formation of clusters and, consequently, should be a step forward in modelling predictions.

5.2. Influence of thermal residual stresses

As evidenced in Fig. 6, the thermal residual stresses do not change damage progression. However, as shown in Fig. 7, they can have a minor influence on the failure and ductile strains. In some material combinations, the failure strain and ductile strain increase when the thermal residual stresses are considered. These changes can be understood as being due to the magnitude of the thermal residual stresses. For the X5-T300 hybrid composites, when $\alpha_{\mathrm{LE}} = 7 \cdot 10^{-6}\ {}^{\circ}C^{-1}$ and $\alpha_{\mathrm{HE}} = -7 \cdot 10^{-6}\ {}^{\circ}C^{-1}$, the HE fibre residual stress is either compressive, or it is tensile albeit smaller than in the other combinations. This, in turn, causes a delay in the initiation of damage for the HE fibre compared to the other scenarios, thus leading to an increase in the failure strain and ductile strain. However, since the magnitude of the thermal stresses is small, the variation in the final failure is very reduced. A similar effect occurs with the X5-Eglass and T300-Eglass composites. When $\alpha_{\mathrm{LE}} = 7 \cdot 10^{-6}\ {}^{\circ}C^{-1}$ and $\alpha_{\mathrm{HE}} = 5 \cdot 10^{-6}\ {}^{\circ}C^{-1}$, smaller residual stresses in the HE fibre are again induced compared to the other combinations when the *HVF* is low. Therefore, either inducing compressive stresses or smaller tensile stresses into the HE fibre should delay the initiation of damage in the HE fibre, leading to an increase in failure strain and ductile strain.

A similar effect is seen with the failure strength and yield stress. This is again controlled by the magnitude of the thermal residual stresses. Introducing compressive stresses into the LE fibre increases the yield stress and failure strength because the initiation of damage in the LE fibre is delayed. This in itself should also increase the hybrid effect, as pointed out in the literature [17, 37, 38].

The results obtained suggest that the thermal residual stresses have a negligible effect on cluster formation and damage evolution. Nonetheless, they can have a minor effect on final failure [6, 17, 38]. Inducing compressive residual stresses for the LE fibre increases the failure strength and yield stress of the material. Likewise, introducing compressive stresses into the HE fibre increases the failure and ductile strains. A combination of the two cases should lead to the best overall behaviour.

6. Conclusions

In this work, a progressive failure model including dynamic effects and thermal residual stresses was developed. The model was used to study the effect the dynamic phenomenon and thermal residual stresses have on the fibre tensile failure process and cluster development of intrayarn hybrid unidirectional composite materials.

Different metrics were used to characterize the failure process of the materials studied: ductile strain, failure strain, yield stress, failure stress, maximum cluster size and the percentage of co-planar clusters. The different hybrids simulated presented a different tensile behaviour, exhibiting a ductile response at low LE hybrid volume fractions. Composites with larger hybrid volume fractions were found to fail in a brittle manner.

The addition of thermal residual stresses had a negligible effect on cluster evolution and damage development. However, they can have some effect on the final failure of the material. Adding compressive residual stresses delays the damage initiation for the LE fibre, leading to an increase in the failure strength and yield stress of the material. That in itself leads to an hybrid effect. Likewise, adding compressive stresses to the HE fibre delays the initiation of damage in the HE fibre, increasing both the failure strain and ductile strain. Combining both scenarios in the right measure should lead to the best overall behaviour.

The dynamic effects were found to have a considerable influence on cluster formation and damage evolution compared to the static model. When the dynamic model was employed, larger clusters were always obtained. Thus, the formation of larger clusters occurred earlier in the dynamic model. This should lead to a more realistic formation of clusters compared to experiments, as was pointed out by Swolfs *et al.* [5]. Nonetheless, the influence on final failure was very minor, with a negligible decrease in failure strain and strength being noted. Despite their minor effect on final failure, a remarkable fact is that some hybrid composites experienced a smaller influence of the dynamic effects compared to the baseline non-hybrid composites, which suggests a small positive hybrid effect caused by the dynamic phenomenon. Therefore, the influence of the dynamic effects on final failure is very dependent on the material system. Although, the impact of the dynamic effect on final failure was negligible, adding dynamic effects should allow a more realistic prediction of cluster formation, thus closing the gap between models and experiments. However, at this point it is impossible to further validate the results from this work due to the lack of experimental data. The literature needs more experimental results, especially with hybrid composites, to be able to improve the available models.

Acknowledgments

The authors acknowledge P.P. Camanho, A.R. Melro and R.P. Tavares for their permission to use their random fibre generator. The authors acknowledge the financial support from the Spanish Ministerio de Economía, Industria y Competitividad (MINECO) under the project TRA2015-71491-R co-financed by the European Regional Development Fund (ERDF). In addition, the authors thank the financial support of the grant RTI2018-097880-B-I00 from the Spanish Ministerio de Ciencia, Innovación y Universidades. The first author also acknowledges the predoctoral Grant BES-2016-078270 from the 'Subprograma Estatal de Formación del MICINN' co-financed by the European Social Fund.

Data availability

The raw/processed data required to reproduce these findings cannot be shared at this time due to legal or ethical reasons.

References

[1] A. Bunsell, L. Gorbatikh, H. Morton, S. Pimenta, I. Sinclair, M. Spearing, Y. Swolfs, A. Thionnet, Benchmarking of strength models for unidirectional composites under longitudinal tension, Composites Part A: Applied Science and Manufacturing 111 (June 2017) (2018) 138–150. doi:10.1016/j.compositesa.2018.03.016.

[2] A. Turon, J. Costa, P. Maimí, D. Trias, J. Mayugo, A progressive damage model for unidirectional fibre-reinforced composites based on fibre fragmentation. Part I: Formulation, Composites Science and Technology 65 (13) (2005) 2039–2048. doi:10.1016/j.compscitech.2005.04.012.

[3] J. Guerrero, J. Mayugo, J. Costa, A. Turon, A 3D Progressive Failure Model for predicting pseudo-ductility in hybrid unidirectional composite materials under fibre tensile loading, Composites Part A: Applied Science and Manufacturing 107 (January) (2018) 579–591. doi:10.1016/j.compositesa.2018.02.005.

[4] J. M. Guerrero, R. P. Tavares, F. Otero, J. A. Mayugo, J. Costa, A. Turon, P. P. Camanho, An analytical model to predict stress fields around broken fibres and their effect on the longitudinal failure of hybrid composites, Composite Structures 211 (December 2018) (2019) 564–576. doi:10.1016/j.compstruct.2018.12.044.

[5] Y. Swolfs, H. Morton, A. E. Scott, L. Gorbatikh, P. A. S. Reed, I. Sinclair, S. M. Spearing, I. Verpoest, Synchrotron radiation computed tomography for experimental validation of a tensile strength model for unidirectional fibre-reinforced composites, Composites Part A: Applied Science and Manufacturing 77 (2015) 106–113. doi:10.1016/j.compositesa.2015.06.018.

[6] Y. Swolfs, L. Gorbatikh, I. Verpoest, Fibre hybridisation in polymer composites: A review, Composites Part A: Applied Science and Manufacturing 67 (2014) 181–200. doi:10.1016/j.compositesa.2014.08.027.

[7] M. R. Wisnom, G. Czel, Y. Swolfs, M. Jalalvand, L. Gorbatikh, I. Verpoest, Hybrid effects in thin ply carbon/glass unidirectional laminates: Accurate experimental de-

termination and prediction, Composites Part A: Applied Science and Manufacturing 88 (2016) 131–139. doi:10.1016/j.compositesa.2016.04.014.

[8] Y. Swolfs, R. M. McMeeking, I. Verpoest, L. Gorbatikh, The effect of fibre dispersion on initial failure strain and cluster development in unidirectional carbon/glass hybrid composites, Composites Part A: Applied Science and Manufacturing 69 (2014) 279–287. doi:10.1016/j.compositesa.2014.12.001.

[9] Y. Swolfs, I. Verpoest, L. Gorbatikh, Maximising the hybrid effect in unidirectional hybrid composites, Materials and Design 93 (2016) 39–45. doi:10.1016/j.matdes.2015.12.137.

[10] Y. Swolfs, R. M. McMeeking, V. P. Rajan, F. W. Zok, I. Verpoest, L. Gorbatikh, Global load-sharing model for unidirectional hybrid fibre-reinforced composites, Journal of the Mechanics and Physics of Solids 84 (2015) 380–394. doi:10.1016/j.jmps.2015.08.009.

[11] R. Tavares, A. R. Melro, M. A. Bessa, A. Turon, W. K. Liu, P. Camanho, Mechanics of hybrid polymer composites: analytical and computational study, Computational Mechanics 57 (3) (2016) 405–421. doi:10.1007/s00466-015-1252-0.

[12] R. Tavares, F. Otero, A. Turon, P. Camanho, Effective simulation of the mechanics of longitudinal tensile failure of unidirectional polymer composites, International Journal of Fracture 208 (1-2) (2017) 269–285. doi:10.1007/s10704-017-0252-9.

[13] G. Czel, T. Rev, M. Jalalvand, M. Fotouhi, M. L. Longana, O. J. Nixon-Pearson, M. R. Wisnom, Pseudo-ductility and reduced notch sensitivity in multi-directional all-carbon/epoxy thin-ply hybrid composites, Composites Part A: Applied Science and Manufacturing 104 (2018) 151–164. doi:10.1016/j.compositesa.2017.10.028.

[14] G. Czel, M. Jalalvand, M. R. Wisnom, Design and characterisation of advanced pseudo-ductile unidirectional thin-ply carbon/epoxy-glass/epoxy hybrid composites, Composite Structures 143 (2016) 362–370. doi:10.1016/j.compstruct.2016.02.010.

[15] H. Yu, M. L. Longana, M. Jalalvand, M. R. Wisnom, K. D. Potter, Pseudo-ductility in intermingled carbon/glass hybrid composites with highly aligned discontinuous

fibres, Composites Part A: Applied Science and Manufacturing 73 (2015) 35–44. doi:10.1016/j.compositesa.2015.02.014.

[16] G. Czel, M. R. Wisnom, Demonstration of pseudo-ductility in high performance glass/epoxy composites by hybridisation with thin-ply carbon prepreg, Composites Part A: Applied Science and Manufacturing 52 (2013) 23–30. doi:10.1016/j.compositesa.2013.04.006.

[17] C. Zweben, Tensile strength of hybrid composites, Journal of Materials Science 12 (7) (1977) 1325–1337. doi:10.1007/BF00540846.

[18] J. Xing, G. Hsiao, T.-W. Chou, A Dynamic Explanation of The Hybrid Effect, Journal of Composite Materials 15 (5) (1981) 443–461. doi:10.1177/002199838101500504.

[19] P. W. Manders, M. G. Bader, The strength of hybrid glass/carbon fibre composites - Part 2 A statistical model, Journal of Materials Science 16 (8) (1981) 2246–2256. doi:10.1007/BF00542387.

[20] J. Hedgepeth, Stress concentrations in filamentary structures, Tech. rep., NASA TN D-882, Nasa report (1961).

[21] J. Xing, X.-R. Liu, T.-W. Chou, Dynamic Stress Concentration Factors in Unidirectional Composites, Journal of Composite Materials 19 (3) (1985) 269–275. doi:10.1177/002199838501900305.

[22] R. Ganesh, S. Sockalingam, B. Z. (Gama) Haque, J. W. Gillespie, Dynamic effects of single fiber break in unidirectional glass fiber-reinforced composites, Journal of Composite Materials 51 (9) (2017) 1307–1320. doi:10.1177/0021998316669218.

[23] R. Ganesh, S. Sockalingam, J. W. Gillespie, Dynamic effects of a single fiber break in unidirectional glass fiber-reinforced polymer composites: Effects of matrix plasticity, Journal of Composite Materials 52 (14) (2018) 1873–1886. doi:10.1177/0021998317737604.

[24] R. P. Tavares, F. Otero, J. Baiges, A. Turon, P. P. Camanho, A dynamic spring element model for the prediction of longitudinal failure of polymer composites, Computational Materials Science 160 (October 2018) (2019) 42–52. doi:10.1016/J.COMMATSCI.2018.12.048.

[25] J. Vanegas, A. Turon, J. Costa, L. Cruz, J. Mayugo, Analytical model for predicting the tensile strength of unidirectional composites based on the density of fiber breaks, Composites Part B: Engineering 141 (February 2017) (2018) 84–91. doi:10.1016/j.compositesb.2017.12.012.

[26] C. Y. Hui, S. Phoenix, M. Ibnabdeljalil, R. L. Smith, An exact closed form solution for fragmentation of Weibull fibers in a single filament composite with applications to fiber-reinforced ceramics, Journal of the Mechanics and Physics of Solids 43 (10) (1995) 1551–1585. doi:10.1016/0022-5096(95)00045-K.

[27] W. A. Curtin, Exact theory of fibre fragmentation in a single-filament composite, Journal of Materials Science 26 (19) (1991) 5239–5253. doi:10.1007/BF01143218.

[28] J. M. Neumeister, A constitutive law for continuous fiber reinforced brittle matrix composites with fiber fragmentation and stress recovery, Journal of the Mechanics and Physics of Solids 41 (8) (1993) 1383–1404. doi:10.1016/0022-5096(93)90085-T.

[29] S. Pimenta, S. T. Pinho, Hierarchical scaling law for the strength of composite fibre bundles, Journal of the Mechanics and Physics of Solids 61 (6) (2013) 1337–1356. doi:10.1016/j.jmps.2013.02.004.

[30] S. Pimenta, A computationally-efficient hierarchical scaling law to predict damage accumulation in composite fibre-bundles, Composites Science and Technology 146 (2017) 210–225. doi:10.1016/j.compscitech.2017.04.018.

[31] T. Okabe, H. Sekine, K. Ishii, M. Nishikawa, N. Takeda, Numerical method for failure simulation of unidirectional fiber-reinforced composites with spring element model, Composites Science and Technology 65 (6) (2005) 921–933. doi:10.1016/j.compscitech.2004.10.030.

[32] A. Thionnet, H. Y. Chou, A. Bunsell, Fibre break processes in unidirectional composites, Composites Part A: Applied Science and Manufacturing 65 (2014) 148–160. doi:10.1016/j.compositesa.2014.06.009.

[33] L. Mishnaevsky, G. Dai, Hybrid carbon/glass fiber composites: Micromechanical analysis of structure-damage resistance relationships, Computational Materials Science 81 (2014) 630–640. doi:10.1016/j.commatsci.2013.08.024.

[34] L. Mishnaevsky, P. Brøndsted, Micromechanisms of damage in unidirectional fiber reinforced composites: 3D computational analysis, Composites Science and Technology 69 (7-8) (2009) 1036–1044. doi:10.1016/j.compscitech.2009.01.022.

[35] G. Bullegas, Carbon Fibre laminates with engineered fracture behaviour, Ph.D. thesis, Imperial College London (2017).

[36] R. P. Tavares, J. M. Guerrero, F. Otero, A. Turon, J. A. Mayugo, J. Costa, P. P. Camanho, Effects of local stress fields around broken fibres on the longitudinal failure of composite materials, International Journal of Solids and Structures 156-157 (2019) 294–305. doi:10.1016/j.ijsolstr.2018.08.027.

[37] P. W. Manders, M. G. Bader, The strength of hybrid glass/carbon fibre composites - Part 1 Failure strain enhancement and failure mode, Journal of Materials Science 16 (8) (1981) 2233–2245. doi:10.1007/BF00542386.

[38] A. R. Bunsell, B. Harris, Hybrid carbon and glass fibre composites, Composites 5 (4) (1974) 157–164. doi:10.1016/0010-4361(74)90107-4.

[39] R. Prussak, D. Stefaniak, C. Hühne, M. Sinapius, Residual Stresses in Intrinsic UD-CFRP-Steel-Laminates - Experimental Determination, Identification of Sources, Effects and Modification Approaches, Materials Science Forum 825-826 (2015) 369–376. doi:10.4028/www.scientific.net/MSF.825-826.369.

[40] H. D. Wagner, Residual Stresses in Microcomposites and Macrocomposites, The Journal of Adhesion 52 (1) (1995) 131–148. doi:10.1080/00218469508015190.

[41] S. Tsai, H. Hahn, Introduction to Composite Materials, Technomic Publishing Co, Inc., 1980.

[42] Y. Swolfs, I. Verpoest, L. Gorbatikh, A review of input data and modelling assumptions in longitudinal strength models for unidirectional fibre-reinforced composites, Composite Structures 150 (2016) 153–172. doi:10.1016/j.compstruct.2016.05.002.

[43] Kelly A., W. Tyson, Tensile properties of fibre-reinforced and metals: copper/tungsten and copper/molybdenum, Journal of the mechanics and physics of solids 13 (6) (1965) 329–350. doi:10.1016/0022-5096(65)90035-9.

[44] L. St-Pierre, N. J. Martorell, S. T. Pinho, Stress redistribution around clusters of broken fibres in a composite, Composite Structures 168 (2017) 226–233. doi:10.1016/j.compstruct.2017.01.084.

[45] H. Cox, The elasticity and strength of paper and other fibrous materials, British Journal of Applied Physics 3 (3) (1952) 72–79. doi:10.1088/0508-3443/3/3/302.

[46] C. M. Landis, R. M. McMeeking, A shear-lag model for a broken fiber embedded in a composite with a ductile matrix, Composites Science and Technology 59 (3) (1999) 447–457. doi:10.1016/S0266-3538(98)00091-8.

[47] A. Eitan, H. D. Wagner, Fiber interactions in two-dimensional composites, Applied Physics Letters 58 (10) (1991) 1033–1035. doi:10.1063/1.105209.

[48] X. F. Zhou, H. D. Wagner, Stress concentrations caused by fiber failure in two-dimensional composites, Composites Science and Technology 59 (7) (1999) 1063–1071. doi:10.1016/S0266-3538(98)00145-6.

[49] A. Arteiro, G. Catalanotti, A. R. Melro, P. Linde, P. P. Camanho, Micro-mechanical analysis of the in situ effect in polymer composite laminates, Composite Structures 116 (1) (2014) 827–840. doi:10.1016/j.compstruct.2014.06.014.

[50] A. R. Melro, P. Camanho, S. T. Pinho, Generation of random distribution of fibres in long-fibre reinforced composites, Composites Science and Technology 68 (9) (2008) 2092–2102. doi:10.1016/j.compscitech.2008.03.013.

[51] G. Kretsis, A review of the tensile, compressive, flexural and shear properties of hybrid fibre-reinforced plastics, Composites 18 (1) (1987) 13–23.

[52] W. Weibull, A statistical distribution function of wide applicability, ASME Journal (1952) 293–297.

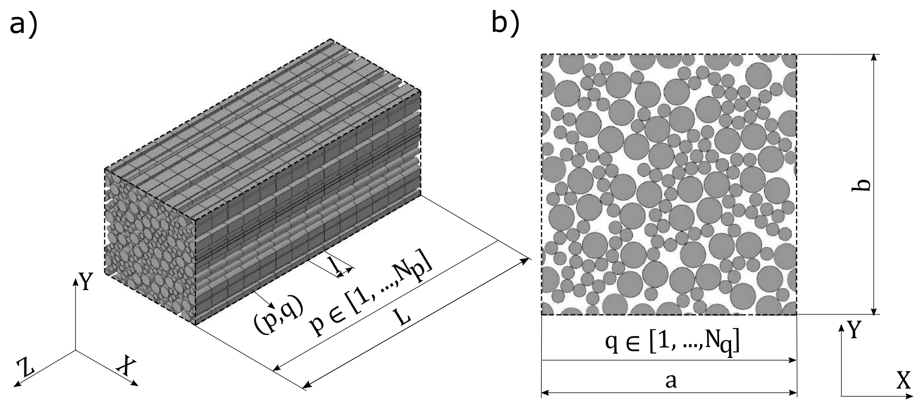

Figure 1: Schema of the RVE employed in the PFM: a) isometric view, b) plane view.

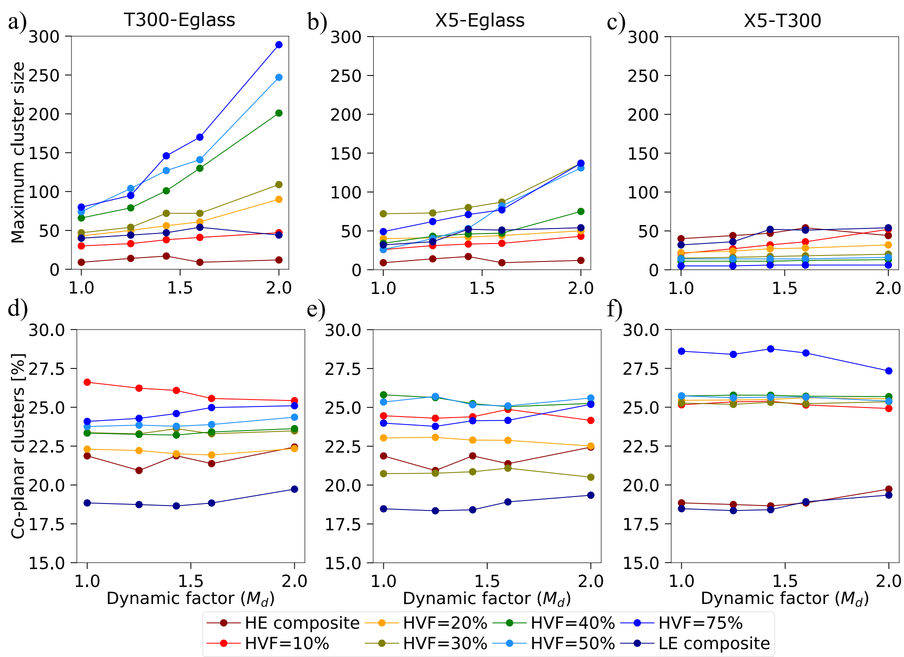

Figure 2: Effect of the dynamic factor on the formation of clusters. From a) to c), the maximum cluster size, in number of broken fibres, is shown within the T300-Eglass, X5-Eglass and X5-T300 composites respectively. From d) to f), the percentage of co-planar clusters are shown within the T300-Eglass, X5-Eglass and X5-T300 composites respectively. The average of 8 runs is shown for each material configuration.

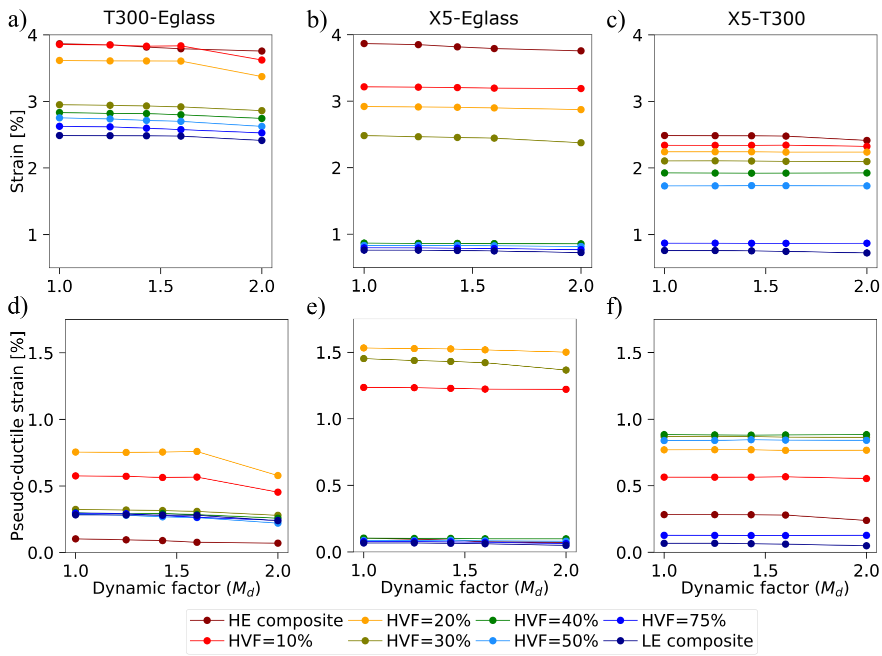

Figure 3: Effect of the dynamic factor on the failure strain and ductile strain. From a) to c), the failure strain is shown within the T300-Eglass, X5-Eglass and X5-T300 composites respectively. From d) to f), the ductile strain is shown within the T300-Eglass, X5-Eglass and X5-T300 composites respectively. The average of 8 runs is shown for each material configuration.

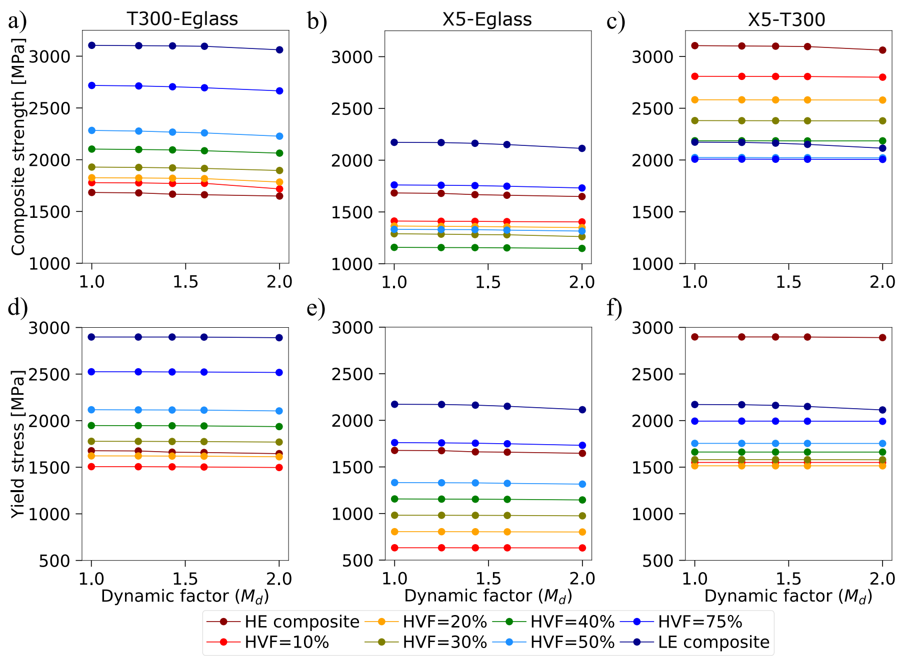

Figure 4: Effect of the dynamic factor on the failure stress and yield stress. From a) to c), the failure stress is shown within the T300-Eglass, X5-Eglass and X5-T300 composites respectively. From d) to f), the yield stress is shown within the T300-Eglass, X5-Eglass and X5-T300 composites respectively. The average of 8 runs is shown for each material configuration.

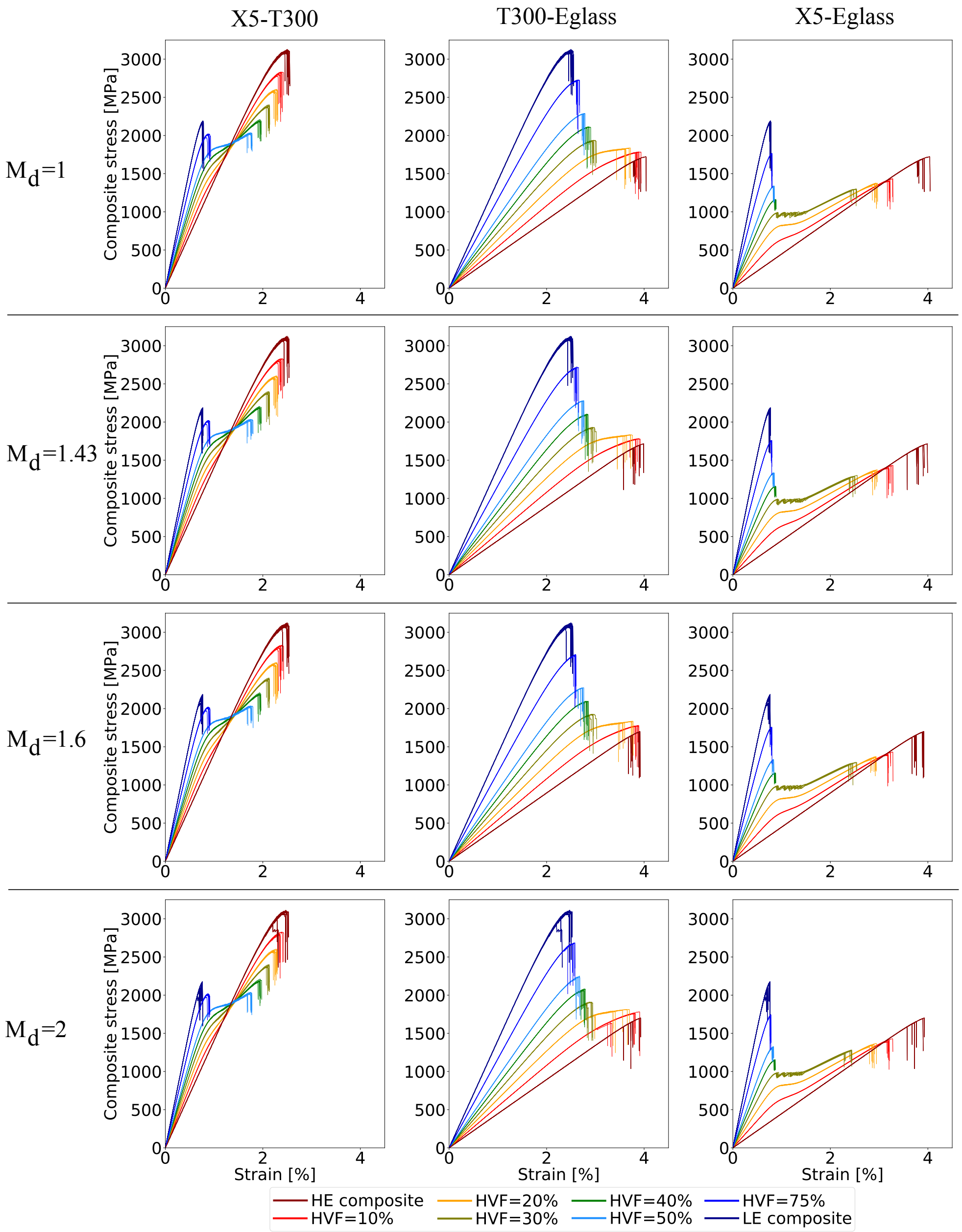

Figure 5: Simulated stress-strain curves with each hybrid composite material for different dynamic factors, M_{d}.

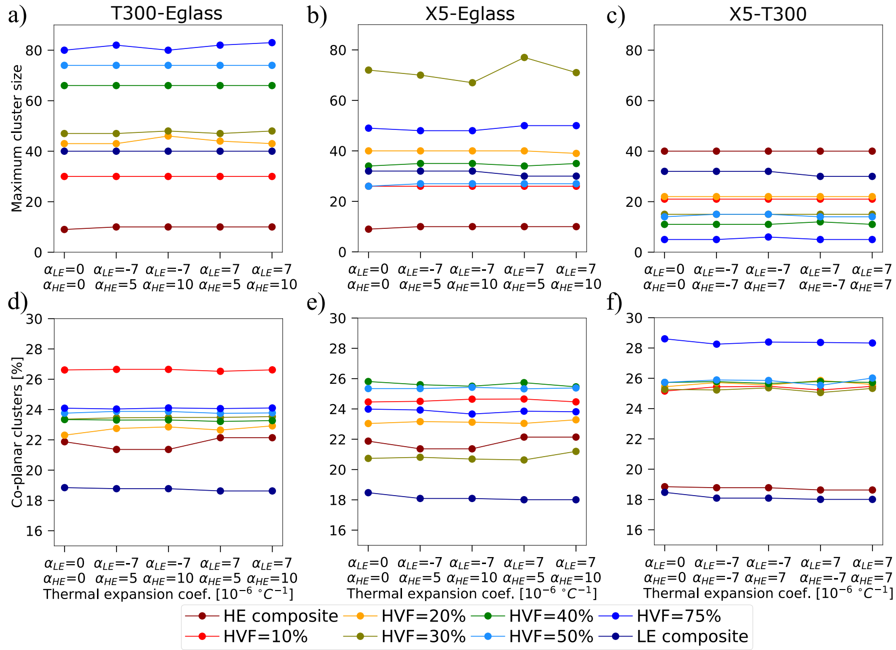

Figure 6: Effect of the thermal residual stresses on the formation of clusters. From a) to c), the maximum cluster size, in number of broken fibres, is shown within the T300-Eglass, X5-Eglass and X5-T300 composites respectively. From d) to f), the percentage of co-planar clusters are shown within the T300-Eglass, X5-Eglass and X5-T300 composites respectively. The average of 8 runs is shown for each material configuration.

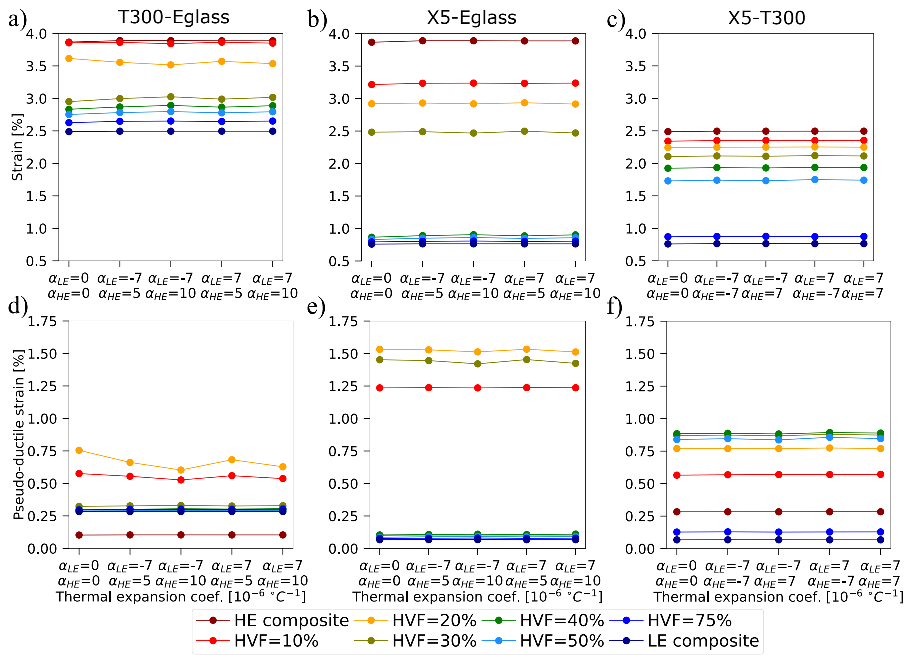

Figure 7: Effect of the thermal residual stresses on the failure strain and ductile strain. From a) to c), the failure strain is shown within the T300-Eglass, X5-Eglass and X5-T300 composites respectively. From d) to f), the ductile strain is shown within the T300-Eglass, X5-Eglass and X5-T300 composites respectively. The average of 8 runs is shown for each material configuration.

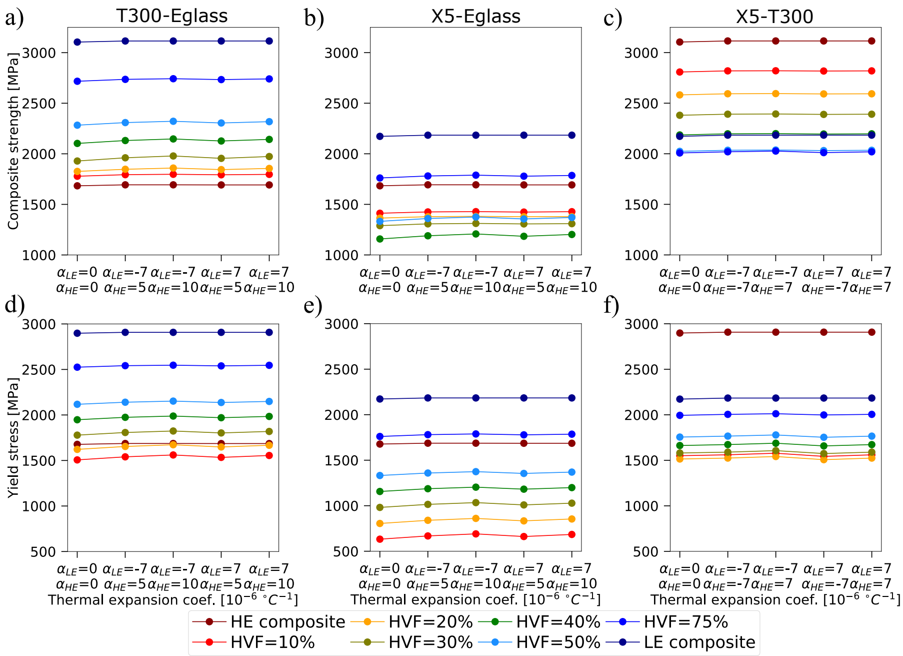

Figure 8: Effect of the thermal residual stresses on the failure stress and yield stress. From a) to c), the failure stress is shown within the T300-Eglass, X5-Eglass and X5-T300 composites respectively. From d) to f), the yield stress is shown within the T300-Eglass, X5-Eglass and X5-T300 composites respectively. The average of 8 runs is shown for each material configuration.

Fibre type	Fibre properties				Weibull parameters		
	E_f [GPa]	R_f [μm]	α_f [$°C^{-1}$] Low	α_f [$°C^{-1}$] High	m [-]	σ_0 [MPa]	L_0 [mm]
T300	232	3.5	$-0.7 \cdot 10^{-6}$	$0.7 \cdot 10^{-6}$	5.10	3170	25
X5	520	5.05	$-0.7 \cdot 10^{-6}$	$0.7 \cdot 10^{-6}$	6.1	2500	25
Eglass	72	8	$5 \cdot 10^{-6}$	$10 \cdot 10^{-6}$	13	2500	25

Table 1: Fibre properties.

Algorithm 1 Progressive Failure Model algorithm

Input: RVE domain and model data (material properties, model options, etc.)

Output: Stress-strain curve, break density, cluster progression, etc.

1: Generate the strength of each element, $\sigma^{\mathrm{u}}_{p,q}$

2: Calculate thermal residual stresses with Eq. (3) if considered

3: Start new step $t + 1$: increase ε^0

4: Start new iteration $y + 1$

5: Estimate $k_{p,q}, k_{p_1}, k_{p_2}, k_p, K, \varepsilon_p$ with Eqs. (5)–(8) using the latest known values of damage, $D_{p,q}$

6: **if** There are broken elements **then**

7:     Calculate $L^{\mathrm{in}}_{p,q}, D_{p,q}$ of broken fibres with Eqs. (10) and (11) if the matrix is plastic, or Eqs. (12) and (13) if it is elastic

8:     Calculate SCF with Eqs. (14)–(19) using the latest known values of $M_{1_{p,c}}$ and $M_{2_{p,c}}$

9:     Re-calculate $k_{p,q}, k_{p_1}, k_{p_2}, k_p, K, \varepsilon_p$ with Eqs. (5)–(8) using the updated values of damage, $D_{p,q}$

10: **end if**

11: Calculate Ω_p and $\sigma_{p,q}$ with Eqs. (4) and (9)

12: **if** Any $\sigma_{p,q} > \sigma^{\mathrm{u}}_{p,q}$ **then**

13:     Set $D_{p,q} = 1$ to all new broken elements

14:     Determine all clusters p, c

15:     For all clusters p, c in which new broken elements of type 1 appeared, $M_{1_{p,c}} = M_{\mathrm{d}}$. For all clusters p, c in which new broken elements of type 2 appeared, $M_{2_{p,c}} = M_{\mathrm{d}}$. For all clusters with no new breaks, $M_{1_{p,c}} = 1$ and $M_{2_{p,c}} = 1$

16:     Start dynamic iteration: go to line 4 if end criteria is not met, otherwise go to line 22

17: **else**

18:     Set all $M_{1_{p,c}} = 1$ and $M_{2_{p,c}} = 1$

19:     Reset iteration counter: $y = 0$

20:     Start new static iteration: go to line 3 if end criteria is not met, otherwise go to line 22

21: **end if**

22: Output simulation data and stop